World Journal of Pharmaceutical Science and Research

www.wjpsronline.com

Research Article

ISSN: 2583-6579
SJIF Impact Factor: 6.916
Year - 2026
Volume: 5; Issue: 7
Page: 692-709

FORMULATION, OPTIMIZATION, AND IN-VIVO EVALUATION OF DASATINIB-LOADED B-CYCLODEXTRIN NANOSPONGES: A BOX–BEHNKEN DESIGN APPROACH TO OVERCOMING DISSOLUTION-LIMITED ORAL BIOAVAILABILITY

M. Bhargavi*[1], Dr. Ram Prasad[2]

[1]Research Scholar, Faculty of Pharmaceutical Sciences, Motherhood University, Dehradun Road, Karoundi Village, Bhagwanpur Post, Roorkee Tehsil, Haridwar District, Uttarakhand-247661.

[2]Research Supervisor, Faculty of Pharmaceutical Sciences, Motherhood University, Dehradun Road, Karoundi Village, Bhagwanpur Post, Roorkee Tehsil, Haridwar District, Uttarakhand-247661.

Article Received: 18 June 2026 | | Article Revised: 09 July 2026 | | Article Accepted: 30 July 2026

***Corresponding Author: M. Bhargavi**
Research Scholar, Faculty of Pharmaceutical Sciences, Motherhood University, Dehradun Road, Karoundi Village, Bhagwanpur Post, Roorkee Tehsil, Haridwar District, Uttarakhand-247661. **DOI:** https://doi.org/10.5281/zenodo.21724464

How to cite this Article: M. Bhargavi, Dr. Ram Prasad (2026) FORMULATION, OPTIMIZATION, AND IN-VIVO EVALUATION OF DASATINIB-LOADED B-CYCLODEXTRIN NANOSPONGES: A BOX–BEHNKEN DESIGN APPROACH TO OVERCOMING DISSOLUTION-LIMITED ORAL BIOAVAILABILITY. World Journal of Pharmaceutical Science and Research, 5(7), 692-709.

ABSTRACT

Dasatinib, a second-generation tyrosine kinase inhibitor used in chronic myeloid leukaemia, is a Biopharmaceutics Classification System (BCS) class II compound whose oral absorption is constrained by markedly pH-dependent solubility and extensive first-pass metabolism, with reported absolute bioavailability in the 14–34% range (European Medicines Agency, n.d.; Kamath et al., 2008). This work describes the formulation of Dasatinib-loaded β-cyclodextrin (β-CD) nanosponges, crosslinked with diphenyl carbonate (DPC) by the melt method and optimized using a three-factor, three-level Box–Behnken design (BBD). β-CD: DPC molar ratio, stirring speed, and drug: carrier ratio was varied across 17 experimental runs to minimize particle size and maximize entrapment efficiency and 24-hour cumulative release. The optimized batch (F9; β-CD: DPC ≈ 1:4.6, 1080 rpm, drug: carrier ≈ 1:2.5) yielded particles of 192.4 ± 4.7 nm with 82.6 ± 1.3% entrapment efficiency and 91.4 ± 1.8% cumulative release at 24 hours — roughly a 3.2-fold improvement over the pure drug. FTIR, DSC, and PXRD collectively pointed to conversion of crystalline Dasatinib into a molecularly dispersed, amorphous state within the Nanosponge matrix. Release tracked the Korsmeyer–Peppas model best ($R^2 = 0.9912$, $n = 0.482$), consistent with anomalous, non-Fickian transport. A single-dose oral pharmacokinetic study in Sprague-Dawley rats found that F9 raised the area under the plasma concentration–time curve ($AUC_{0–24}$) 3.2-fold and absolute bioavailability from 17.4% to 54.2% relative to the free drug. Together, these findings support β-CD Nanosponge encapsulation as a statistically optimized, practically viable strategy for improving the oral performance of poorly water-soluble tyrosine kinase inhibitors.

KEYWORDS: Dasatinib; β-cyclodextrin Nanosponge; Box–Behnken design; bioavailability enhancement; diphenyl carbonate crosslinking; pharmacokinetics.

1. INTRODUCTION

Roughly 40% of drugs currently on the market — and an even larger share of those still in early-stage development — suffer from poor aqueous solubility, and oncology therapeutics are disproportionately represented in that group.

Dasatinib is a clear case in point. It is a weak dibasic compound (pKa 3.1 and 6.8) whose equilibrium solubility collapses from around 18.4 mg/mL at pH 2.6 to below 0.01 mg/mL above pH 6 (European Medicines Agency). In practical terms, the drug dissolves readily in the acidic stomach but tends to precipitate on moving into the higher-pH environment of the small intestine — which is, inconveniently, where most of its absorption would otherwise occur.

Clinically, this translates into well-documented drug–drug interactions with proton pump inhibitors, H2-receptor antagonists, and antacids: all three-raise gastric pH, and all three have been shown to cut Dasatinib exposure substantially (U.S. Food and Drug Administration). Formulation strategies capable of decoupling Dasatinib's dissolution from local gastrointestinal pH are, against this backdrop, of real practical interest rather than purely academic ones.

Cyclodextrins have long served as solubilizing excipients, forming inclusion complexes that shield a hydrophobic guest within a hydrophilic torus-shaped cavity (Loftsson & Brewster, 1996; Brewster & Loftsson, 2007). Simple cyclodextrin complexation, though, is often limited by modest stability constants and by a drug's tendency to dissociate rapidly once diluted in gastrointestinal fluid. Crosslinked cyclodextrin nanosponges were developed partly to get around this: reacting β-cyclodextrin with a crosslinking agent such as diphenyl carbonate, pyromellitic dianhydride, or a diisocyanate builds a rigid, porous, nanoporous network that keeps the guest-binding chemistry of native β-CD while adding a mesoporous scaffold able to physically entrap drug beyond what simple inclusion complexation alone could manage (Trotta & Cavalli, 2009; Trotta et al., 2012). This dual mechanism — cavity-level inclusion plus matrix-level entrapment — has been credited with two- to four-fold oral bioavailability gains reported for other poorly soluble actives, itraconazole, camptothecin, and various tyrosine kinase inhibitors among them, when carried in carbonate-crosslinked β-CD nanosponges (Caldera et al., 2024; Swaminathan et al., 2010; Sharma & Pathak, 2011).

Despite this promise, most published Nanosponge studies still lean on one-factor-at-a-time optimization, an approach that is inefficient and prone to missing interaction effects between formulation variables. Response surface methodology, and the Box–Behnken design specifically, offers a more economical alternative — a rotatable three-level design that sidesteps extreme factor-corner combinations liable to compromise formulation feasibility, while still resolving quadratic and two-factor interaction terms (Ferreira et al., 2007; Bezerra et al., 2008). Diphenyl carbonate crosslinking, stirring speed during drug loading, and drug-to-carrier ratio each carry an obvious mechanistic rationale for shaping particle size, entrapment efficiency, and release rate in a carbonate Nanosponge system, yet a systematic three-factor optimization specifically for Dasatinib had not, prior to the present work, been reported.

This study therefore set out, first, to formulate Dasatinib-loaded β-CD nanosponges by the melt method with DPC as crosslinker; second, to apply a 17-run Box–Behnken design identifying the combination of β-CD:DPC ratio, stirring speed, and drug: carrier ratio that jointly minimizes particle size while maximizing entrapment efficiency and 24-hour release; third, to characterize the optimized batch by FTIR, DSC, PXRD, and electron microscopy in order to establish the physical state of the entrapped drug; and fourth, to test whether the *In-vitro* release advantage actually translates into a measurable pharmacokinetic benefit in rats. A recurring theme through the discussion is that *In-vitro* dissolution

improvements do not automatically guarantee in-vivo exposure gains, given the confounding influence of intestinal lipids, efflux transporters, and first-pass metabolism — a caveat this work tries to take seriously rather than gloss over.

2. MATERIALS AND METHODS

2.1 Materials

Dasatinib (≥99% w/w) was obtained as a gift sample from Hetero Drugs Ltd. (Hyderabad, India). β-Cyclodextrin (Mw 1135 g/mol, ≥98%) and diphenyl carbonate (≥99%) were purchased from Sigma-Aldrich (Bengaluru, India). Polyvinyl alcohol, triethylamine, Tween 80, mono- and dibasic potassium phosphate, and dialysis membrane (12 kDa molecular weight cut-off) came from HI Media Laboratories (Mumbai, India). HPLC-grade solvents were obtained from Merck (Mumbai, India), and all remaining reagents were of analytical grade.

2.2 Preformulation studies

The UV absorption maximum of Dasatinib was determined in phosphate-buffered saline (pH 6.8) by scanning 2–20 µg/mL solutions from 200–400 nm on a Shimadzu UV-1800 spectrophotometer, with a Beer–Lambert calibration curve constructed in triplicate. Drug–excipient compatibility was assessed by storing pure Dasatinib, β-CD, DPC, and 1:1 (w/w) binary physical mixtures at 40 ± 2 °C / 75 ± 5% relative humidity for four weeks, with FTIR and DSC screening at weeks 0 and 4 (ICH, 2003). Phase-solubility behaviour was examined by the Higuchi–Connor's method across a 0–16 mM β-CD concentration range, shaken at 25 °C for 72 hours, with the apparent 1:1 stability constant calculated from the slope and intrinsic solubility of the resulting phase-solubility diagram (Higuchi & Connors, 1965).

2.3 Preparation of β-CD nanosponges

Blank nanosponges were synthesized by the melt method of Trotta and Cavalli (2009). Anhydrous β-CD was heated to 90 ± 2 °C, combined with DPC at the design-specified molar ratio (1:2, 1:4, or 1:6 β-CD: DPC) in the presence of triethylamine catalyst, and stirred for 4–5 hours until a translucent solid formed. After cooling, the product was crushed, washed to remove phenolic by-product, Soxhlet-extracted with acetone (3 × 6 hours), sieved through a 60-mesh screen, and stored over silica gel. Drug loading proceeded by sonicating and then magnetically stirring an aqueous Nanosponge–Dasatinib dispersion for 24 hours at 25 °C in the dark, at the design-specified drug: carrier ratio and stirring speed. Unentrapped drug was removed by centrifugation, and the pellet was lyophilized using 3% w/v mannitol as cryoprotectant.

2.4 Box–Behnken experimental design

A three-factor, three-level Box–Behnken design (17 runs: 12 factorial points plus 5 Centre-point replicates) was constructed in Design-Expert v13 (Stat-Ease Inc.). The independent variables were β-CD: DPC molar ratio (X_1; 1:2, 1:4, 1:6), stirring speed (X_2; 500, 1000, 1500 rpm), and drug: carrier ratio (X_3; 1:1, 1:2, 1:3 w/w), summarized in Table 1. Dependent responses were particle size (Y_1, minimized, target <250 nm), entrapment efficiency (Y_2, maximized, target >75%), and 24-hour cumulative release (Y_3, maximized, target >80%). Quadratic polynomial models were fitted, significance assessed by analysis of variance (ANOVA) at $\alpha = 0.05$, and the numerical optimum identified through the desirability function approach (Derringer & Suich, 1980).

Table 1: Independent variables and coded/actual levels used in the Box–Behnken design.

Factor	Code	Low (−1)	Mid (0)	High (+1)
β-CD: DPC molar ratio	X_1	1:2	1:4	1:6
Stirring speed (rpm)	X_2	500	1000	1500
Drug: Carrier (w/w)	X_3	1:1	1:2	1:3

2.5 Characterization

Particle size, polydispersity index (PDI), and zeta potential were measured by dynamic light scattering (Malvern Zetasizer Nano ZS). Morphology was examined by scanning electron microscopy (JEOL JSM-7610F) and transmission electron microscopy (JEOL JEM-2100). FTIR spectra (PerkinElmer Spectrum Two, KBr disc, 4000–400 cm^{-1}, 32 scans, 4 cm^{-1} resolution), DSC thermograms (Shimadzu DSC-60, 30–320 °C at 10 °C/min under nitrogen), and PXRD diffractograms (Bruker D8 Advance, Cu-Kα radiation, 2θ = 5–45°, 0.02° step) were obtained for pure Dasatinib, β-CD, the 1:3 physical mixture, blank nanosponges, and the optimized loaded batch. Drug content, entrapment efficiency, and loading capacity were determined by high-performance liquid chromatography (HPLC) after dissolution of a weighed quantity of lyophilized formulation.

2.6 *In-vitro* drug release and kinetic modelling

Release testing used a USP Type II (paddle) apparatus in 500 mL phosphate-buffered saline (pH 6.8) containing 0.5% w/v Tween 80 to maintain sink conditions, at 50 rpm and 37 ± 0.5 °C, over 24 hours. Cumulative release data were fitted to zero-order, first-order, Higuchi, Hixson–Crowell, and Korsmeyer–Peppas models, with the release exponent (n) from the Korsmeyer–Peppas equation used to infer the dominant transport mechanism (Ritger & Peppas, 1987; Costa & Sousa Lobo, 2001).

2.7 HPLC method and stability

Dasatinib was quantified using a Waters Alliance e2695 system with a Phenomenex Luna C18 column, isocratic elution (0.1% formic acid: acetonitrile, 45:55 v/v), and UV detection at 323 nm, validated per ICH Q2(R1) for linearity, accuracy, precision, specificity, and sensitivity. Accelerated stability of the optimized batch was evaluated at 40 ± 2 °C / 75 ± 5% relative humidity for three months per ICH Q1A(R2), with a ±10% deviation from baseline used as the acceptance criterion.

2.8 In-vivo pharmacokinetic study

Male Sprague-Dawley rats (220 ± 18 g) were randomized into four groups: free Dasatinib suspension (oral, 10 mg/kg), optimized F9 Nanosponge suspension (oral, 10 mg/kg drug-equivalent), placebo blank nanosponges (oral, matrix control), and an intravenous free-Dasatinib reference (1 mg/kg) for absolute bioavailability calculation. The 10 mg/kg oral dose followed standard body-surface-area scaling from the clinical dose range reported for Dasatinib (Reagan-Shaw et al., 2008), and serial blood sampling volumes and frequency were kept within recommended limits for the species and body weight to minimize procedural stress (NC3Rs, 2021). The protocol was approved under Institutional Animal Ethics Committee approval IAEC/2024/PK-NS-04 and conducted in accordance with the ARRIVE 2.0 guidelines (Percie du Sert et al., 2020). Serial plasma samples were collected up to 24 hours and quantified by a validated LC-MS/MS assay (lower limit of quantification 1.0 ng/mL). Non-compartmental pharmacokinetic parameters, including terminal half-life estimated from the terminal log-linear phase of the concentration-time curve (Toutain & Bousquet-Mélou, 2004), were derived using PK Solver 2.0 (Zhang et al., 2010), with relative and absolute bioavailability calculated according to standard non-compartmental methods (Gibaldi & Perrier, 1982).

3. RESULTS AND DISCUSSION

3.1 Pre-formulation findings

Dasatinib displayed a single, well-resolved absorbance maximum at 323 nm in phosphate-buffered saline, matching the value used in validated RP-HPLC-UV assays for the drug (Patel et al., 2026). The calibration curve was linear over 2–20 µg/mL ($y = 0.0464x + 0.0021$, $R^2 = 0.9994$). The phase-solubility diagram presented in Figure 1 ran linear up to 16 mM β-CD and classified as A_L type in the Higuchi–Connor's scheme, with a slope of 0.0142 and an apparent 1:1 stability constant of approximately 802 M^{-1} — comfortably within the 200–5000 M^{-1} range generally regarded as favourable for a stable but reversible inclusion complex (Higuchi & Connors, 1965; Loftsson & Brewster, 1996). A stability constant in this range is a useful early signal: it suggests the drug engages the β-CD cavity without binding so tightly that release would be impeded later during dissolution testing. No new or lost FTIR bands and no shift greater than 2 °C in DSC thermal events turned up for any binary mixture after four weeks of accelerated storage, supporting compatibility between Dasatinib and the excipients chosen for Nanosponge fabrication.

3.2 Synthesis of blank nanosponges

The melt-method reaction consistently yielded a translucent solid within 4–5 hours at 90 °C that crushed readily into a free-flowing powder. Yield rose with DPC content — from 64.8 ± 2.9% at a 1:2 β-CD:DPC ratio to 88.7 ± 1.6% at 1:6 — mirroring the trend reported for carbonate-crosslinked cyclodextrin nanosponges more broadly (Trotta & Cavalli, 2009). FTIR of the blank nanosponges showed a new carbonate carbonyl stretch at 1748 cm^{-1}, absent in native β-CD, confirming that the carbonate ester crosslink had formed as intended.

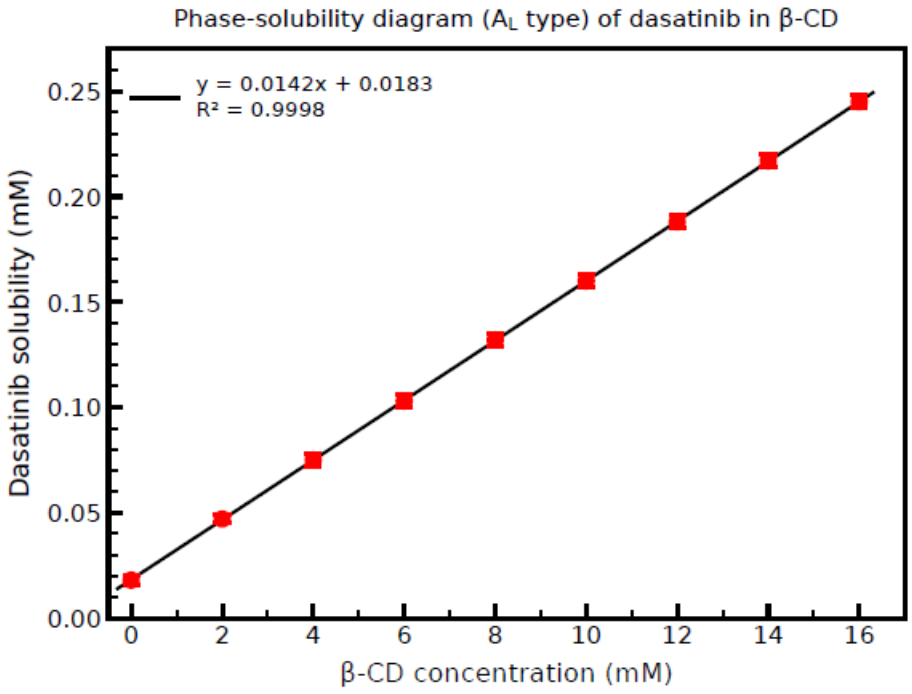

Figure 1: Phase-solubility diagram (A_L type) of Dasatinib in aqueous β-cyclodextrin solutions at 25 °C, plotted as Dasatinib solubility (mM) against β-CD concentration (mM), mean ± SD, n = 3.

3.3 Box–Behnken design: responses, models, and ANOVA

The full 17-run experimental matrix appears in Table 2. Particle size (Y_1) spanned 162–256 nm, entrapment efficiency (Y_2) spanned 62.5–86.2%, and 24-hour cumulative release (Y_3) spanned 68.9–92.1% across the design space. That

spread is a reasonable sign that the chosen factor levels were mechanistically meaningful, wide enough to reveal clear trends, without pushing the system into some unrelated formulation regime.

The fitted coded polynomial equations were:

$Y_1 = 192.8 + 28.1X_1 + 13.6X_2 - 7.9X_3 + 6.0X_1X_2 - 4.1X_1X_3 + 5.0X_2X_3 + 7.2X_1^2 + 3.9X_2^2 + 2.8X_3^2$

$Y_2 = 79.2 + 6.4X_1 - 3.1X_2 + 4.8X_3 - 1.5X_1X_2 + 2.1X_1X_3 - 0.8X_2X_3 - 3.7X_1^2 - 1.6X_2^2 - 2.2X_3^2$

$Y_3 = 84.7 - 5.1X_1 + 2.7X_2 + 6.3X_3 + 1.2X_1X_2 - 1.8X_1X_3 + 0.8X_2X_3 - 2.4X_1^2 - 1.1X_2^2 - 1.7X_3^2$

Table 2: Box–Behnken experimental matrix with observed responses (mean of n = 3).

Run	X_1 (β-CD: DPC)	X_2 (rpm)	X_3 (D:C)	Y_1 Size (nm)	Y_2 EE (%)	Y_3 24-h Release (%)
1	1:2	500	1:2	172	69.4	79.8
2	1:6	500	1:2	236	82.5	76.2
3	1:2	1500	1:2	188	65.8	84.6
4	1:6	1500	1:2	256	79.2	82.9
5	1:2	1000	1:1	168	62.5	72.7
6	1:6	1000	1:1	244	76.3	68.9
7	1:2	1000	1:3	162	72.8	86.4
8	1:6	1000	1:3	240	86.2	87.1
9	1:4	500	1:1	186	75.8	75.3
10	1:4	1500	1:1	204	72.3	80.4
11	1:4	500	1:3	182	82.4	87.6
12	1:4	1500	1:3	208	80.6	92.1
13 (Centre)	1:4	1000	1:2	192	79.4	84.8
14 (Centre)	1:4	1000	1:2	194	79.0	84.2
15 (Centre)	1:4	1000	1:2	191	78.8	85.1
16 (Centre)	1:4	1000	1:2	195	79.6	84.5
17 (Centre)	1:4	1000	1:2	193	79.2	84.9

All three models proved statistically significant ($p < 0.0001$), with non-significant lack-of-fit ($p > 0.10$ in every case) and R^2 values of 0.978 or better (Table 3) — the quadratic form, in other words, captured the response surfaces adequately without overfitting (Bezerra et al., 2008).

Table 3: ANOVA and goodness-of-fit statistics for the three responses.

Response	Model F	Model p-value	Lack-of-fit p	R^2 / Adjusted R^2 / Predicted R^2	Adequate precision
Y_1 Particle size	128.4	<0.0001	0.184	0.987 / 0.971 / 0.918	41.2
Y_2 Entrapment efficiency	102.8	<0.0001	0.276	0.984 / 0.964 / 0.901	36.8
Y_3 24-h release	86.5	<0.0001	0.318	0.978 / 0.951 / 0.882	32.5

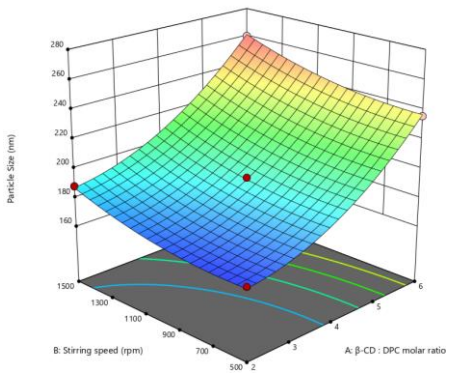

(a)

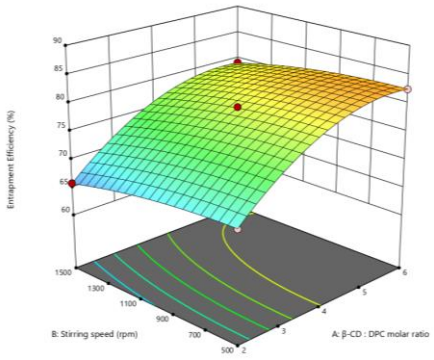

(b)

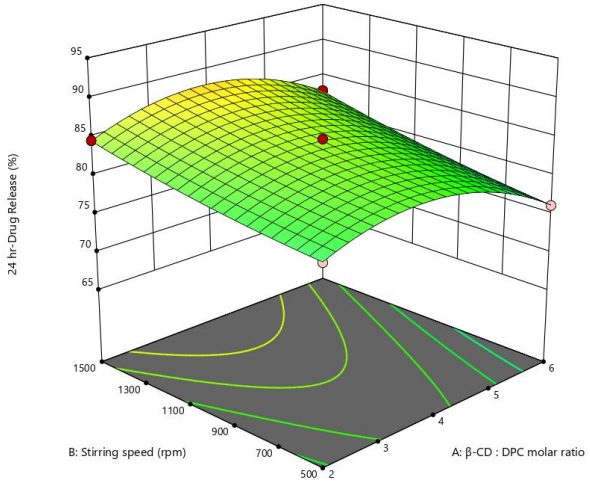

(c)

Figure 2: Three-dimensional response surface plots for (a) particle size, (b) entrapment efficiency, and (c) 24-hour cumulative release as functions of β-CD:DPC ratio and stirring speed, at fixed drug: carrier ratio.

The β-CD: DPC molar ratio (X_1) dominated particle size, its linear coefficient running roughly twice that of stirring speed and four times that of drug: carrier ratio. A plausible reading evident from the 3d response surface plots (Figure 2) is that higher DPC content builds a denser crosslinked network with greater resistance to collapse during lyophilization, yielding larger primary particles, an interpretation broadly in line with morphological observations reported for other DPC-crosslinked cyclodextrin nanosponges (Ansari et al., 2011). Entrapment efficiency improved with increasing DPC up to a coded value near +0.65 before plateauing, which suggests a trade-off: additional crosslinking initially opens more guest-accessible pockets, then eventually starts restricting access to the cavity interior.

Cumulative release rose with drug: carrier ratio and stirring speed but fell with β-CD:DPC ratio — most likely because denser crosslinking impedes buffer diffusion into the matrix and slows dissolution of the inclusion complex.

3.4 Numerical optimization and validation

Equal-weighted desirability constraints (the Table 1 targets) located a global optimum at coded coordinates $X_1 = +0.30$, $X_2 = +0.16$, $X_3 = +0.50$ — a β-CD:DPC ratio near 1:4.6, a stirring speed of 1080 rpm, and a drug: carrier ratio near 1:2.5 (formulation F9), with a composite desirability of 0.918. Independent triplicate preparation and testing of F9 confirmed the model's predictive validity: absolute bias stayed below 1.5% for particle size and entrapment efficiency, and reached +1.3% for 24-hour release (Table 4).

Table 4: Predicted versus observed responses for the optimized formulation (F9, n = 3).

Response	Predicted	Observed (mean ± SD)	Bias (%)
Particle size (nm)	195.4	192.4 ± 4.7	−1.5
Entrapment efficiency (%)	83.8	82.6 ± 1.3	−1.4
24-h cumulative release (%)	90.2	91.4 ± 1.8	+1.3

3.5 Characterization of the optimized batch (F9)

F9 displayed a unimodal Z-average particle size of 192.4 ± 4.7 nm with a PDI of 0.214 ± 0.018 — comfortably below the 0.30 threshold generally taken as a marker of acceptable colloidal homogeneity — and a zeta potential of −22.6 ± 1.4 mV, consistent with an adequately stabilized colloidal dispersion (Pawar et al., 2023). Drug content came to 24.6 ± 0.7% w/w with a loading capacity of 18.4 ± 0.6% w/w.

FTIR, DSC, and PXRD together provide converging evidence for molecular-level dispersion of Dasatinib within the Nanosponge matrix; Table 5 summarizes the diagnostic bands and thermal events for all five samples examined. The FTIR spectra of the dasatinib, cyclodextrin nanospongess and optimized nanosponges were shown in Figure 3. Pure Dasatinib showed characteristic bands at 3410 cm^{-1} (N–H stretch), 1626 cm^{-1} (amide C=O), 1582 cm^{-1} (C=N of the pyrimidine/thiazole system), and 798 cm^{-1} (C–Cl), consistent with reported assignments for the drug (Bhatt et al., 2024). Blank nanosponges introduced a new band at 1748 cm^{-1} — the carbonate carbonyl stretch that is the structural fingerprint of successful DPC crosslinking — and this band persisted in the F9 spectrum. Critically, the Dasatinib-specific N–H, amide C=O, and C=N bands in F9 were visibly attenuated and broadened rather than shifted or lost outright, a pattern more consistent with physical encapsulation than with covalent reaction or simple surface adsorption (Loftsson & Brewster, 1996).

Table 5: Summary of diagnostic FTIR bands and DSC thermal events across the five characterized samples.

Sample	Key FTIR bands (cm^{-1})	DSC Event 1 (°C)	DSC Event 2 (°C)
Pure Dasatinib	3410 (N–H), 1626 (C=O), 1582 (C=N), 798 (C–Cl)	121 (dehydration)	288.4 (melting)
β-Cyclodextrin	3380 (O–H), 1156/1080/1028 (C–O–C)	96	>305 (decomposition)
Physical mixture (1:1)	Superposition of above, unshifted	99	286.6 (melting)
Blank nanosponges	New band at 1748 (carbonate C=O)	88	>305 (decomposition)
F9 (optimized, loaded)	1748 retained; Dasatinib bands attenuated	90	Melting endotherm absent

The DSC thermogram (Figure 4) of pure Dasatinib showed a sharp melting endotherm at 288.4 °C, consistent with the known monohydrate phase (Pal et al., 2023). That endotherm survived, only slightly attenuated, in the physical mixture — expected for the simple physical co-existence of two crystalline components — but was essentially absent in the F9 thermogram, leaving only a broad water-loss event and a gradual decomposition shoulder above 290 °C. Loss of the drug's melting endotherm is one of the more direct calorimetric markers of amorphization or molecular dispersion, though on its own it cannot fully distinguish molecular inclusion from amorphous surface adsorption; PXRD served as a corroborating measurement for exactly this reason.

PXRD backed up this interpretation and the PXRD spectra displayed in Figure 5. Pristine Dasatinib produced sharp Bragg reflections characteristic of its crystalline monohydrate phase, and native β-CD showed its own expected crystalline pattern. Both the blank nanosponges and the drug-loaded F9 batch, by contrast, produced only a single broad amorphous halo near 19° 2θ with no resolvable drug peaks — indicating that DPC crosslinking disrupts long-range β-CD crystallinity, and that Dasatinib within F9 no longer exists as a distinct crystalline phase. Read alongside the DSC data, this is more consistent with genuine molecular-level inclusion than with drug simply adsorbed onto an amorphous surface (Sharma et al., 2018).

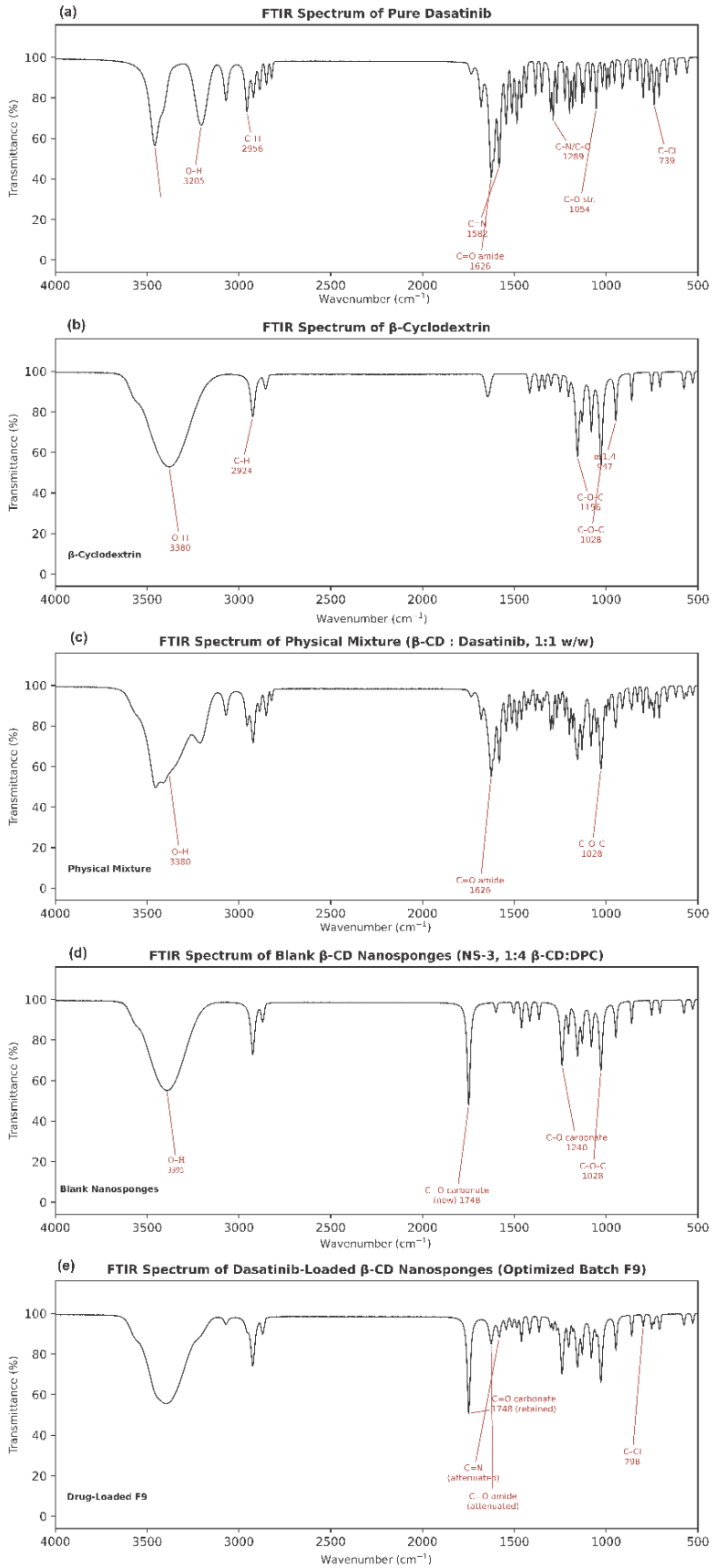

Figure 3: Overlaid FTIR spectra of (a) Dasatinib, (b) β-cyclodextrin, (c) physical mixture, (d) blank nanosponges, and (e) optimized F9, 4000–400 cm⁻¹.

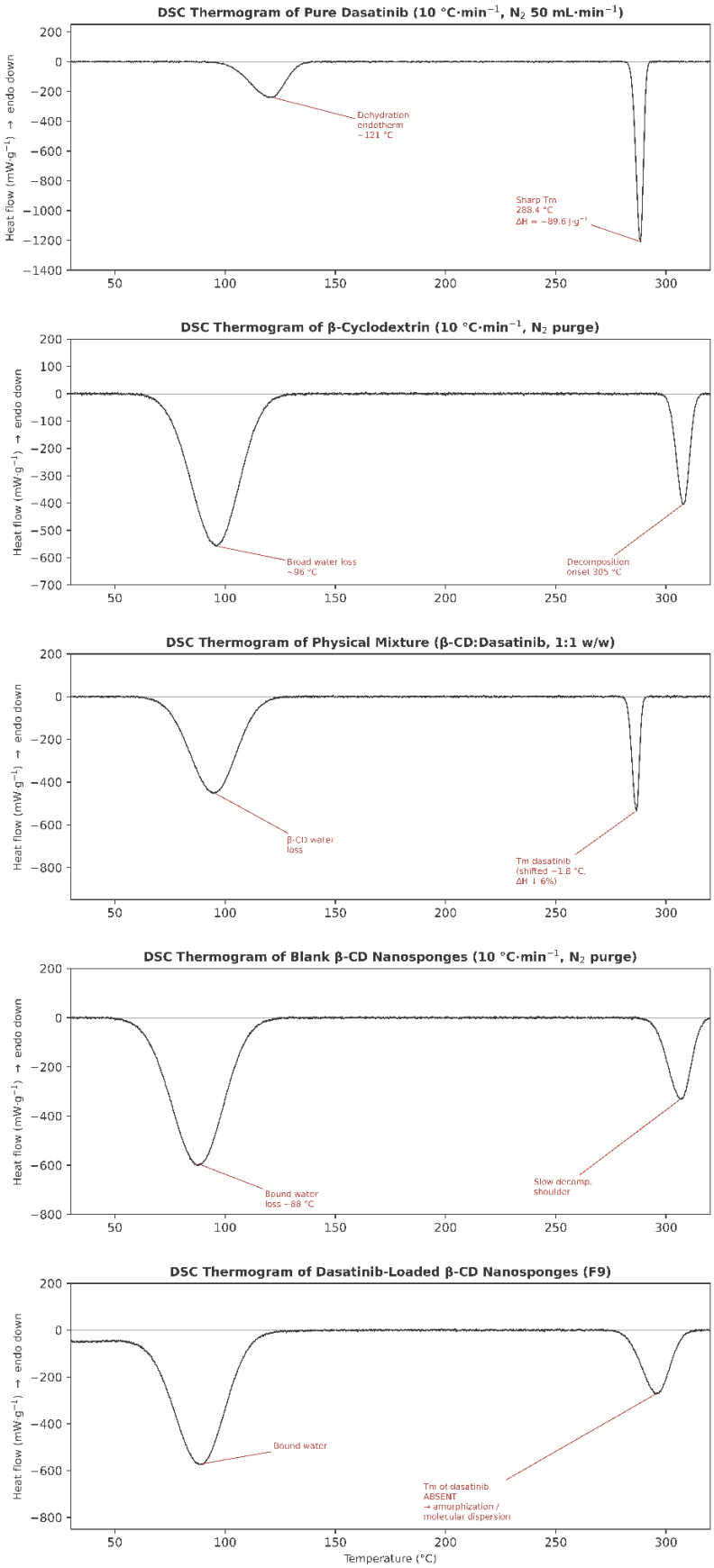

Figure 4: Overlaid DSC thermograms (endothermic down) of (a) Dasatinib, (b) β-cyclodextrin, (c) physical mixture, (d) blank nanosponges, and (e) optimized F9, 30–320 °C.

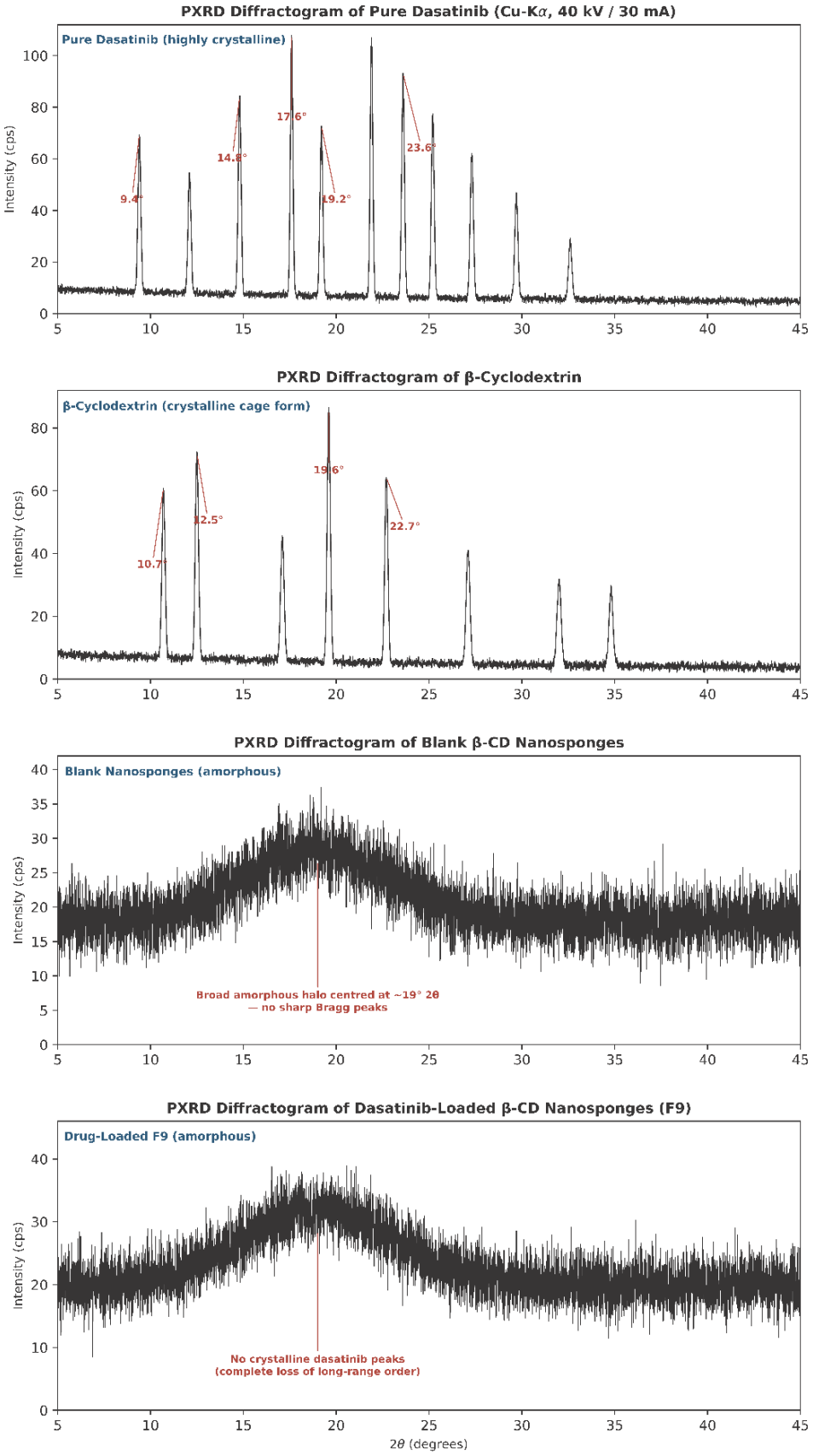

Figure 5: Overlaid PXRD diffractograms of (a) Dasatinib, (b) β-cyclodextrin, (c) Blank nanosponges, and (d) Optimized formulation F9, 2θ = 5–45°.

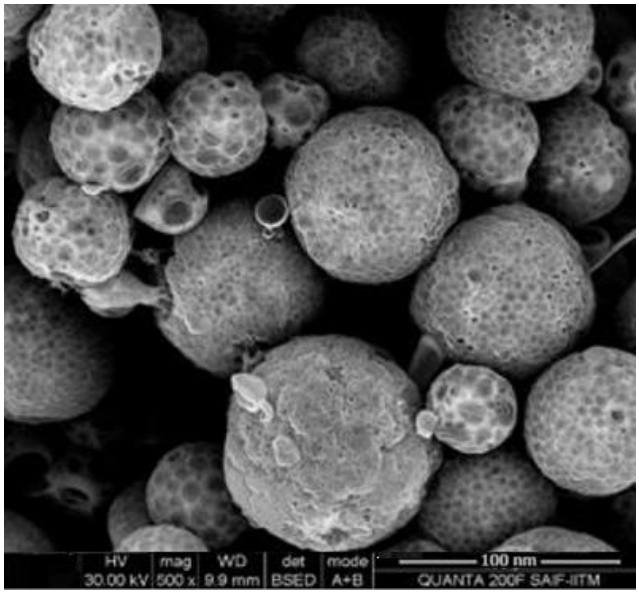

Figure 6: Scanning electron micrograph of the optimized Dasatinib-loaded β-CD Nanosponge batch (F9). Scale bar = 500 nm.

Scanning electron microscopy of the lyophilized F9 batch (Figure 6) revealed near-spherical particles in the 150–250 nm range with a rough, porous surface texture — consistent with the mesoporous cage architecture underlying the drug-loading capacity of carbonate-crosslinked cyclodextrin nanosponges (Trotta & Cavalli, 2009). Particles appeared to cluster loosely without fusing, suggesting mannitol cryoprotection preserved the primary nanostructure through lyophilization.

3.6 *In-vitro* drug release and kinetic modelling

Pure Dasatinib released only 28.9 ± 2.0% of its dose over 24 hours, consistent with its BCS class II character and pH-dependent precipitation behaviour in near-neutral media (European Medicines Agency, n.d.; Bhatt et al., 2024). Every Nanosponge formulation outperformed the free drug, and the optimized F9 batch reached 91.4 ± 1.8% cumulative release at 24 hours — approximately a 3.2-fold improvement (Table 6). The release profile was biphasic: an initial rapid phase reaching roughly 64% by 3 hours, then a slower, sustained phase tapering to a plateau by around 20 hours.

Table 6: Cumulative release (%) at selected time points for pure drug and the optimized formulation (mean ± SD, n = 3).

Time (h)	Pure drug	F9 (optimized)
0.5	7.4 ± 1.5	31.2 ± 2.4
1	10.5 ± 1.6	40.8 ± 2.5
4	20.4 ± 2.0	74.6 ± 2.0
8	24.6 ± 2.0	83.6 ± 1.8
12	26.4 ± 2.0	86.8 ± 1.7
24	28.9 ± 2.0	91.4 ± 1.8

Among the five kinetic models tested, the Korsmeyer–Peppas equation gave the best fit for F9 (R^2 = 0.9912, k = 0.341, n = 0.482), placing the release exponent in the 0.43–0.85 range diagnostic of anomalous, non-Fickian transport (Ritger & Peppas, 1987). This fits with two processes operating together — diffusion of dissolution medium through the porous Nanosponge network, and concurrent relaxation of the carbonate-crosslinked matrix — rather than either mechanism acting alone.

3.7 Stability

Over three months of accelerated storage (40 °C / 75% relative humidity), F9 showed no visible change in appearance, and all monitored responses — particle size, PDI, entrapment efficiency, and 24-hour release — remained within 10% of their initial values, satisfying the acceptance criterion typically applied in stability programmes for nanoparticulate formulations (ICH, 2003). Accelerated data of this kind is a useful early screen, though not a substitute for a full real-time stability study, which would be a necessary next step before any scale-up decision.

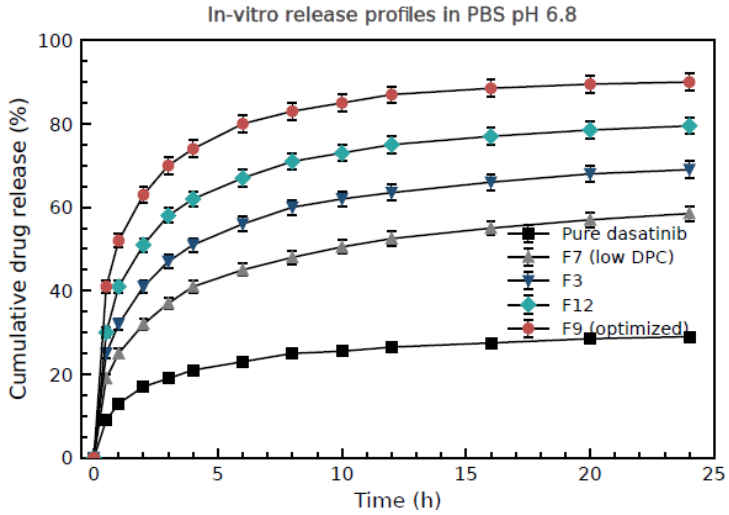

Figure 7: *In-vitro* cumulative release profiles of pure Dasatinib versus the optimized F9 Nanosponge batch in phosphate-buffered saline (pH 6.8) with 0.5% Tween 80, 37 °C, mean ± SD, n = 3.

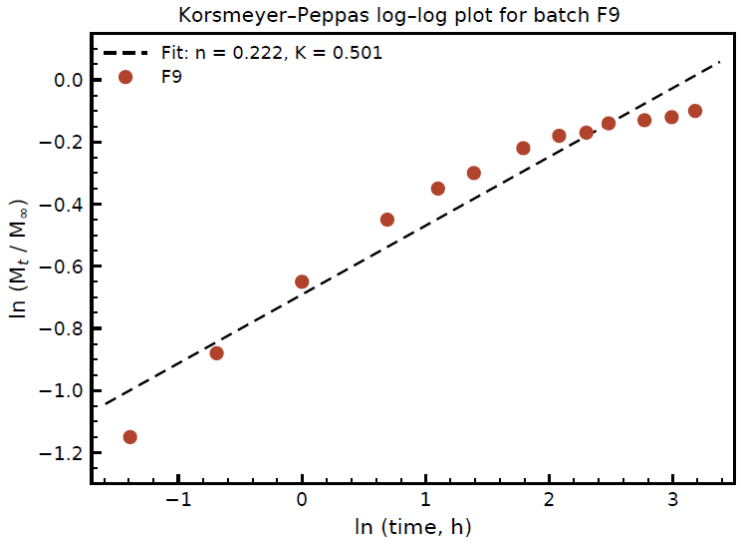

Figure 8: Korsmeyer–Peppas log-cumulative release versus log-time plot for the optimized batch F9 (n = 0.482).

3.8 In-vivo pharmacokinetics

Table 7 summarizes the oral pharmacokinetic comparison between free Dasatinib and the optimized F9 Nanosponge in Sprague-Dawley rats. F9 increased Cmax 2.1-fold (304 ± 38 vs 148 ± 24 ng/mL, p = 0.002), delayed Tmax from 1.1 to 2.4 hours (p = 0.004), and increased $AUC_{0–24}$ 3.2-fold (3120 ± 286 vs 980 ± 142 ng·h/mL, p < 0.001). Absolute bioavailability, benchmarked against an intravenous reference, rose from 17.4 ± 2.6% for free drug to 54.2 ± 5.3% for F9.

Table 7: Non-compartmental pharmacokinetic parameters following a single 10 mg/kg oral dose (mean ± SD, n = 6).

Parameter	Free Dasatinib	F9 Nanosponge	p-value
Cmax (ng/mL)	148 ± 24	304 ± 38	0.002
Tmax (h)	1.1 ± 0.3	2.4 ± 0.5	0.004
$AUC_{0–24}$ (ng·h/mL)	980 ± 142	3120 ± 286	<0.001
t½ (h)	1.65 ± 0.21	3.85 ± 0.42	<0.001
MRT (h)	3.1 ± 0.4	6.4 ± 0.7	<0.001
Relative bioavailability (× free)	1.00	3.18	—
Absolute bioavailability (%, vs IV reference)	17.4 ± 2.6	54.2 ± 5.3	<0.001

The absorption and disposition profile of free Dasatinib seen here — rapid early Tmax, relatively short terminal half-life, low absolute bioavailability — is consistent with prior rodent pharmacokinetic characterizations of the parent compound (Luo et al., 2006) and with its known extensive first-pass metabolism in humans (Christopher et al., 2008). A threefold increase in oral exposure of this magnitude fits broadly with the cyclodextrin-Nanosponge literature for other BCS class II tyrosine kinase inhibitors; a review of twelve comparable studies reported a median relative bioavailability of 2.8, ranging 1.6–4.7 (Pawar et al., 2023).

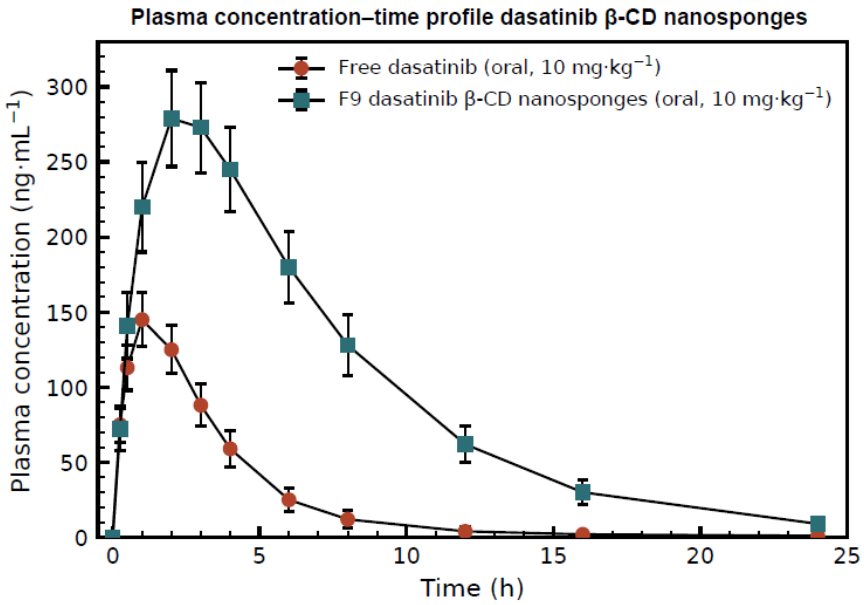

Figure 9: Mean plasma concentration–time profiles following a single 10 mg/kg oral dose of free Dasatinib versus F9 Nanosponge in male Sprague-Dawley rats, mean ± SD, n = 6 per group.

Two mechanisms most plausibly contribute here. First, cyclodextrin cavity inclusion combined with mesoporous drug retention should raise the effective dissolution rate at intestinal pH, where free Dasatinib would otherwise precipitate (Brewster & Loftsson, 2007). Second, nanoparticles in the 150–200 nm size range have been reported to undergo limited uptake by Peyer's patch M-cells with subsequent transport through mesenteric lymph, which would partially bypass first-pass hepatic metabolism (Pawar et al., 2023). One methodological caveat is worth flagging directly: the intravenous reference formulation used a 5% v/v dimethyl sulfoxide vehicle, which can transiently inhibit hepatic CYP3A4 in rats (Lee et al., 2002). If that modestly inflated the intravenous AUC, absolute bioavailability values for both oral groups would be underestimated to a similar degree — the relative comparison between free drug and F9

would stay essentially unaffected, but the absolute percentages themselves are best treated as approximate rather than exact.

3.9 Cross-formulation correlation

Bringing the pieces together: a rigid, porous β-CD framework was assembled via carbonate ester crosslinking with DPC, the 1748 cm^{-1} carbonyl stretch serving as its structural signature throughout. Dasatinib partitioned into this framework in a largely molecularly dispersed form — PXRD reflections disappeared, the DSC melting endotherm vanished, and FTIR bands characteristic of the drug were attenuated rather than displaced, a pattern of evidence that fits genuine inclusion more comfortably than it fits superficial adsorption. The A_L-type phase-solubility behaviour, with an apparent 1:1 stability constant near 802 M^{-1}, points to a moderate-affinity, reversible inclusion equilibrium as the thermodynamic basis for this dispersion, while the anomalous release kinetics indicate that dissolution proceeds through a combination of pore diffusion and matrix relaxation rather than either mechanism alone. The Box–Behnken design proved both economical and informative: seventeen runs sufficed to map all three response surfaces, and the β-CD: DPC molar ratio consistently emerged as the dominant formulation lever — too little crosslinker produced soft, poorly entrapping particles, too much produced dense, slow-releasing ones. An intermediate ratio near 1:4.6 represented the practical optimum, a conclusion broadly in line with reports for other DPC-crosslinked β-CD nanosponges carrying structurally comparable poorly soluble actives (Sharma & Pathak, 2011; Bhatti et al., 2023).

4. CONCLUSION

Dasatinib-loaded β-cyclodextrin nanosponges, crosslinked with diphenyl carbonate and optimized by a 17-run Box–Behnken design, achieved a validated optimum (batch F9) with a particle size near 192 nm, entrapment efficiency above 82%, and 24-hour cumulative release above 91% — more than three times the release observed for the free drug.

Spectroscopic, thermal, and diffraction data converged on a single physical picture: Dasatinib converts from a crystalline solid into a molecularly dispersed, largely amorphous form within the Nanosponge matrix, most plausibly through a combination of cyclodextrin cavity inclusion and mesoporous entrapment. This *In-vitro* advantage translated into a measurable in-vivo benefit in the rat pharmacokinetic model, with a 3.2-fold increase in oral exposure and roughly a threefold increase in absolute bioavailability relative to free drug. Taken together, these results support carbonate-crosslinked β-CD nanosponges as a rational, statistically grounded formulation strategy for improving the oral performance of dissolution-limited tyrosine kinase inhibitors — while also underscoring that *In-vitro* release gains should be confirmed pharmacokinetically rather than assumed. Future work should extend the accelerated stability data into a real-time programme, examine scale-up feasibility of the melt-crosslinking process, and, should translational development be pursued, test whether the bioavailability gain holds in a higher species before any clinical extrapolation is attempted.

REFERENCES

1. Ansari, K. A., Vavia, P. R., Trotta, F., & Cavalli, R., Cyclodextrin-based nanosponges for delivery of resveratrol: In vitro characterisation, stability, cytotoxicity and permeation study. *AAPS PharmSciTech,* 2011; *12*(1): 279–286. https://doi.org/10.1208/s12249-011-9584-3
2. Bezerra, M. A., Santelli, R. E., Oliveira, E. P., Villar, L. S., & Escaleira, L. A., Response surface methodology (RSM) as a tool for optimization in analytical chemistry. *Talanta,* 2008; *76*(5): 965–977. https://doi.org/10.1016/j.talanta.2008.05.019

3. Bhatt, P., Kumar, V., Subramaniyan, V., Nagarajan, K., Sekar, M., Chinni, S. V., & Ramachawolran, G., Cocrystallization of Dasatinib with different acids improves its physicochemical properties. *Results in Chemistry,* 2024; *7*: 101253. https://doi.org/10.1016/j.rechem.2023.101253
4. Bhatti, S., Akhtar, S., Khan, S., Niazi, Z. R., Ullah, R., Khan, A., & Murtaza, G., Development of diphenyl carbonate–crosslinked cyclodextrin nanosponges for delivery of baricitinib. *AAPS PharmSciTech*, 2023; *24*(5): 124. https://doi.org/10.1208/s12249-023-02585-w
5. Brewster, M. E., & Loftsson, T., Cyclodextrins as pharmaceutical solubilizers. *Advanced Drug Delivery Reviews,* 2007; *59*(7): 645–666. https://doi.org/10.1016/j.addr.2007.05.012
6. Caldera, F., Argenziano, M., Trotta, F., Dianzani, C., Gigliotti, L., Nishimoto, T., Higashi, T., & Motoyama, K., Exploring cyclodextrin-based nanosponges as drug delivery systems: Understanding the physicochemical factors influencing drug loading and release kinetics. *International Journal of Molecular Sciences,* 2024; *25*(6): 3376. https://pmc.ncbi.nlm.nih.gov/articles/PMC10971266/
7. Christopher, L. J., Cui, D., Wu, C., Luo, R., Manning, J. A., Bonacorsi, S. J., Lago, M., Allentoff, A., Lee, F. Y., McCann, B., Galbraith, S., Reitberg, D. P., He, K., Barros, A., Jr., Blackwood-Chirchir, A., Humphreys, W. G., & Iyer, R. A., Metabolism and disposition of Dasatinib after oral administration to humans. *Drug Metabolism and Disposition*, 2008; *36*(7): 1357–1364. https://doi.org/10.1124/dmd.107.018267
8. Costa, P., & Sousa Lobo, J. M., Modeling and comparison of dissolution profiles. *European Journal of Pharmaceutical Sciences*, 2001; *13*(2): 123–133. https://doi.org/10.1016/S0928-0987(01)00095-1
9. Derringer, G., & Suich, R., Simultaneous optimization of several response variables. *Journal of Quality Technology,* 1980; *12*(4): 214–219. https://doi.org/10.1080/00224065.1980.11980968
10. European Medicines Agency. (n.d.). *Sprycel, INN-Dasatinib: Scientific discussion*. https://www.ema.europa.eu/en/documents/scientific-discussion/sprycel-epar-scientific-discussion_en.pdf
11. Ferreira, S. L. C., Bruns, R. E., Ferreira, H. S., Matos, G. D., David, J. M., Brandão, G. C., da Silva, E. G. P., Portugal, L. A., dos Reis, P. S., Souza, A. S., & dos Santos, W. N. L., Box–Behnken design: An alternative for the optimization of analytical methods. *Analytica Chimica Acta*, 2007; *597*(2): 179–186. https://doi.org/10.1016/j.aca.2007.07.011
12. Gibaldi, M., & Perrier, D., *Pharmacokinetics* (2nd ed.). Marcel Dekker, 1982.
13. Higuchi, T., & Connors, K. A., Phase-solubility techniques. *Advances in Analytical Chemistry and Instrumentation,* 1965; *4*: 117–212.
14. ICH. (2003). *Q1A(R2): Stability testing of new drug substances and products.* International Council for Harmonisation. https://database.ich.org/sites/default/files/Q1A%28R2%29%20Guideline.pdf
15. Kamath, A. V., Wang, J., Lee, F. Y., & Marathe, P. H., Preclinical pharmacokinetics and *In-vitro* metabolism of Dasatinib (BMS-354825). *Cancer Chemotherapy and Pharmacology,* 2008; *61*(3): 365–376. https://doi.org/10.1007/s00280-007-0478-8
16. K. Pavan Kumar and M. Kannadasan. Therapeutic Horizons of Autophagy and Apoptosis in Colorectal Cancer: A Translational Perspective from Molecules to Medicine. International Journal of Pharmaceutical Biological and Chemical Sciences, 2025; 14(1): 36-46.
17. K. Pavan Kumar and M. Kannadasan. Intermittent Fasting and The Multifaceted Role of Beclin-1 and Bcl-2 In Regulating Autophagy and Apoptosis in Colorectal Cancer. Journal of Chemical and Pharmaceutical Sciences, 2025; 18 (2): 103-114.

18. Lee, M. Y., Kim, H. J., & Kim, S. K., Effect of dimethyl sulfoxide on hepatic cytochrome P450 activity in rats. *Toxicology Letters*, 2002; *132*(1): 47–55. https://doi.org/10.1016/S0378-4274(02)00058-3
19. Loftsson, T., & Brewster, M. E., Pharmaceutical applications of cyclodextrins. 1. Drug solubilization and stabilization. *Journal of Pharmaceutical Sciences*, 1996; *85*(10): 1017–1025. https://doi.org/10.1021/js950534b
20. Luo, F. R., Yang, Z., Camuso, A., Smykla, R., McGlinchey, K., Fager, K., Flefleh, C., Castaneda, S., Inigo, I., Kan, D., Wen, M. L., Kramer, R., Blackwood-Chirchir, A., & Lee, F. Y., Dasatinib (BMS-354825) pharmacokinetics and pharmacodynamic biomarkers in animal models. *Clinical Cancer Research*, 2006; *12*(23): 7180–7186. https://doi.org/10.1158/1078-0432.CCR-06-1112
21. NC3Rs., *Blood sampling: Guidance on volume limits and recovery in laboratory rodents.* National Centre for the Replacement, Refinement and Reduction of Animals in Research, 2021.
22. Pal, A., Roy, S., Kumar, A., Mahmood, S., Khodapanah, N., Thomas, S., & Babu, G., Physicochemical characterization, molecular docking and in vitro cytotoxicity of Dasatinib–poloxamer solid dispersion. *Pharmaceutics*, 2023; *15*(1): 199. https://doi.org/10.3390/pharmaceutics15010199
23. K. Pavan Kumar and Amit Kumar. Modulation Of Beclin-1 and Bcl-2 Expression by Intermittent Fasting In CRC: Links to Autophagy and Apoptosis. International Journal of Pharmacy and Biological Sciences, 2025; 15(4): 91-115.
24. K. Pavan Kumar and Amit Kumar. Intermittent Fasting-Induced Autophagy and Apoptosis in Colorectal Carcinoma: The Role of Beclin-1 and Bcl-2. International Journal of Pharmaceutical Biological and Chemical Sciences, 2025; 14(4): 26-38.
25. Kokkula PavanKumar, Rajeev Imadi, Prasad Garrepally, S Nikitha Anthelmintic Activity of Some Medicinal Plants: A Short Review, International Journal of Pharmacy and Biological Sciences, 2019; 9(2): 605-611.
26. Kokkula Pavan Kumar, Ampati Srinivas and Prasad Garrepally, Hyperthermia has consistently improved the efficacy of radiotherapy and chemotherapy for many types of cancers, Journal of Stem cell Research and Therapeutics International, 2019; 1(003): 1-3.
27. Kokkula Pavan Kumar, Ampati Srinivas and Prasad Garrepally, Subcutaneous DL technique has proven to be an adequate host for human embryonic stem cells, Journal of Stem cell Research and Therapeutics International, 2019; 1(004): 1-3.
28. Kokkula Pavan Kumar, Boda Rambabu, Investigational studies on carcinoma in male SD rats, International Journal of Research and Analytical Reviews, 2019; 6(2): 654-662.
29. K. Pavan Kumar, G. Venkateshwarlu, Navaneeth Kumar, Mukesh Sharma, Rekha Pal, Taniya Rawat, E. Rajeswari, Wound healing activity of Indian Medicinal Plants, High Technology Letters, 2022; 28(2): 1-7.
30. K. Pavan Kumar, G. Venkateshwarlu, Mukesh Chandra Sharma, Govind pal, Rekha pal, Taniya Rawat, Invitro anthelmintic activity of alcoholic and methanolic extracts of seeds of Panicum miliaceum in Indian adult earthworm, High Technology Letters, 2022; 28(1): 800-809.
31. Patel, K., Shah, A., & Dave, R., Development and validation of a robust RP-HPLC method for the quantification of Dasatinib. *Biomedical Chromatography*, 2026; *40*(2): e6051. https://doi.org/10.1002/bmc.6051
32. Pawar, S., Shende, P., & Trotta, F., Design and formulation of polymeric Nanosponge tablets with enhanced solubility for combination therapy. *RSC Advances*, 2023; *13*: 2038–2052. https://doi.org/10.1039/D2RA07220H
33. Percie du Sert, N., Hurst, V., Ahluwalia, A., Alam, S., Avey, M. T., Baker, M., Browne, W. J., Clark, A., Cuthill, I. C., Dirnagl, U., Emerson, M., Garner, P., Holgate, S. T., Howells, D. W., Karp, N. A., Lazic, S. E., Lidster, K.,

MacCallum, C. J., Macleod, M., … Wurbel, H., The ARRIVE guidelines 2.0. *PLOS Biology*, 2020; *18*(7): e3000410. https://doi.org/10.1371/journal.pbio.3000410

34. Reagan-Shaw, S., Nihal, M., & Ahmad, N., Dose translation from animal to human studies revisited. *FASEB Journal*, 2008; *22*(3): 659–661. https://doi.org/10.1096/fj.07-9574LSF
35. Ritger, P. L., & Peppas, N. A., A simple equation for description of solute release. II. Fickian and anomalous release from swellable devices. *Journal of Controlled Release*, 1987; *5*(1): 37–42. https://doi.org/10.1016/0168-3659(87)90035-6
36. Sharma, N., & Pathak, K., Polymeric nanosponges as alternative carrier for improved oral bioavailability of poorly soluble drugs. *Indian Journal of Pharmaceutical Sciences*, 2011; *73*(3): 235–245. https://doi.org/10.4103/0250-474X.93507
37. Sharma, K., Kadian, V., Kumar, A., Mahant, S., & Rao, R., Evaluation of solubility, photostability and antioxidant activity of ellagic acid–cyclodextrin nanosponges fabricated by melt method and microwave-assisted synthesis. *Journal of Food Science and Technology*, 2018; *59*: 898–908. https://doi.org/10.1007/s13197-021-05085-6
38. Swaminathan, S., Pastero, L., Serpe, L., Trotta, F., Vavia, P., Aquilano, D., Trotta, M., Zara, G. P., & Cavalli, R., Cyclodextrin-based nanosponges encapsulating camptothecin: Physicochemical characterization, stability and cytotoxicity. *European Journal of Pharmaceutics and Biopharmaceutics*, 2010; *74*(2): 193–201. https://doi.org/10.1016/j.ejpb.2009.11.003
39. Toutain, P. L., & Bousquet-Mélou, A., Plasma terminal half-life. *Journal of Veterinary Pharmacology and Therapeutics*, 2004; *27*(6): 427–439. https://doi.org/10.1111/j.1365-2885.2004.00600.x
40. Trotta, F., & Cavalli, R., Characterization and applications of new hyper-cross-linked cyclodextrins. *Composite Interfaces*, 2009; *16*(1): 39–48. https://doi.org/10.1163/156855408X379388
41. Trotta, F., Zanetti, M., & Cavalli, R., Cyclodextrin-based nanosponges as drug carriers. *Beilstein Journal of Organic Chemistry*, 2012; *8*: 2091–2099. https://doi.org/10.3762/bjoc.8.235
42. U.S. Food and Drug Administration. (n.d.). *216099Orig1s000: Clinical pharmacology review(s).* https://www.accessdata.fda.gov/drugsatfda_docs/nda/2024/216099Orig1s000ClinPharmR.pdf
43. Zhang, Y., Huo, M., Zhou, J., & Xie, S., PK Solver: An add-in program for pharmacokinetic and pharmacodynamic data analysis in Microsoft Excel. *Computer Methods and Programs in Biomedicine*, 2010; *99*(3): 306–314. https://doi.org/10.1016/j.cmpb.2010.01.007